coatings

MDPI

Article

Performance Evaluation and Thermal Shock Behavior of PS-PVD $(Gd_{0.9}Yb_{0.1})_2Zr_2O_7$/YSZ Thermal Barrier Coatings

Hongxu Zhao [1,2], Xiaofeng Zhang [2], Chunming Deng [2], Ziqian Deng [2,*] and Xiaolong Chen [1,*]

[1] Institute of Advanced Wear & Corrosion Resistant and Functional Materials, Jinan University, Guangzhou 510632, China; hongxu_zhao@163.com
[2] National Engineering Laboratory for Modern Materials Surface Engineering Technology, Institute of New Materials, Guangdong Academy of Science, Guangzhou 510650, China; zxf200808@126.com (X.Z.); denghans@163.com (C.D.)
* Correspondence: dengziqian@gdinm.com (Z.D.); xiaolong.chen@jnu.edu.cn (X.C.)

Abstract: In this study, $(Gd_{0.9}Yb_{0.1})_2Zr_2O_7$ (GYbZ)/yttria-stabilized zirconia (YSZ) double-ceramic-layer (DCL) thermal barrier coatings (TBCs) were prepared by plasma spray-physical vapor deposition (PS-PVD). The microstructure, mechanical performance, and thermal shock behavior of coatings prepared with spraying distances of 600, 800, and 1000 mm were investigated. The GYbZ coating prepared with a spraying distance of 600 mm showed a closely packed columnar structure. However, the GYbZ coatings prepared with spraying distances of 800 and 1000 mm showed a quasi-columnar structure. The GYbZ coating prepared with a spraying distance of 800 mm had the thickest columnar crystals with obvious inter-columnar gaps. In addition, this coating exhibited excellent mechanical performance and the best thermal shock resistance. The primary failure patterns appearing during thermal shocking on the surface of TBCs can be classified into the following five types: caves, exfoliation, delamination cracks, spalled areas, and radiate cracks. Furthermore, the failure behavior of these coatings in water-quenching tests is clarified.

Keywords: TBC; PS-PVD; spraying distance; failure behavior

Citation: Zhao, H.; Zhang, X.; Deng, C.; Deng, Z.; Chen, X. Performance Evaluation and Thermal Shock Behavior of PS-PVD $(Gd_{0.9}Yb_{0.1})_2Zr_2O_7$/YSZ Thermal Barrier Coatings. *Coatings* **2022**, *12*, 323. https://doi.org/10.3390/coatings12030323

Academic Editors: Stefano Caporali and Emanuele Galvanetto

Received: 24 January 2022
Accepted: 17 February 2022
Published: 1 March 2022

1. Introduction

Thermal barrier coatings (TBCs) are increasingly employed to protect the underlying metal substrate in various products [1,2], such as gas turbines and aero-engines. TBCs are usually deposited on parts exposed to high temperatures to decrease fuel consumption and improve thermal efficiency [3]. Recently, with the development of gas turbines, TBC materials must exhibit enhanced high-temperature behaviors due to higher inlet temperatures [4]. Among the various promising ultra-high-temperature TBC materials, gadolinium zirconate ($Gd_2Zr_2O_7$; GZO) has received increasing attention due to its superior stability and insulation properties at elevated temperatures [5,6]. However, it has some shortcomings, such as poor fracture toughness and a mismatched thermal expansion coefficient with substrates, resulting in several problems, including insufficient bonding strength and a short thermal cycling life of the GZO coatings [7]. Their thermophysical properties can be improved by substituting the Gd or Zr sites in GZO materials with other rare-earth cations [8]. In addition, to prolong the TBCs' thermal cycle life, a double-ceramic-layer (DCL) coating system was proposed [9] to alleviate the thermal expansion coefficient mismatch between the metal bond coat and ceramic layer. Guo et al. [10] explored the thermophysical properties of Yb_2O_3-doped $Gd_2Zr_2O_7$ ($(Gd_{1-x}Yb_x)_2Zr_2O_7$ (x = 0, 0.1, 0.3, 0.5, and 0.7)) and reported that the thermal conductivity of $(Gd_{0.9}Yb_{0.1})_2Zr_2O_7$ (GYbZ) is the lowest among the investigated samples. Further, the electron-beam physical vapor deposition (EB-PVD) technique was employed to prepare yttria-stabilized zirconia (YSZ)/GYbZ DCL TBCs. The thermal cycle tests showed that the average service life of the TBCs exceeded 3700 cycles.

In general, TBCs are prepared using EB-PVD or air plasma spraying (APS) techniques [11]. The APS technique can quickly prepare coatings with lamellar structures, showing good thermal insulation performance but poor thermal shock resistance. On the other hand, the EB-PVD technique can prepare coatings with columnar structures, which possess high-strain tolerance but insufficient thermal insulation [12,13]. In recent years, a promising novel technology, plasma spray-physical vapor deposition (PS-PVD), has attracted significant attention from the research community. The PS-PVD technique has the combined advantages of the EB-PVD and APS techniques and can produce coatings containing various structures to meet the growing needs of advanced gas turbines [14]. Recently, several reports have been published on TBCs' preparation and deposition patterns using the PS-PVD technique, whereby different coating structures, such as mixed, columnar, and layered, can be prepared by adjusting process conditions, for example, feed rate and spraying distance [15,16]. Among these coating structures, the gas-phase deposited quasi-columnar coating is attractive for TBCs owing to its excellent strain tolerance and low thermal conductivity in thermal cycles [17,18]. For instance, Li et al. [19] prepared YSZ coatings using the PS-PVD technique with spraying distances of 450–1400 mm. They obtained quasi-columnar structure coatings when the spraying distance was greater than 600 mm. In addition, Zhang et al. [20] explored the deposition mechanisms of the PS-PVD technique and developed a model for nucleation and coating growth processes.

In this study, GYbZ/YSZ DCL TBCs were prepared using the PS-PVD technique. To study the variations in microstructure and coating performance with spraying distance, GYbZ ceramic layers were deposited by varying spraying distances from 600 to 1000 mm. The coatings' microstructure was observed using field emission-scanning electron microscope (FE-SEM), and thermal shock resistance was evaluated by water-quenching tests. Finally, we determined the effects of spraying distance on the microstructure and thermal shock behavior of TBCs.

2. Materials and Methods

2.1. TBC Preparation

A PS-PVD system (Oerlikon Metco, Winterthur, Switzerland) equipped with a single cathode O3CP gun was used to prepare the TBCs. The raw materials were 7YSZ powders (M6700 Oerlikon Metco, Winterthur, Switzerland) and GYbZ powders that were synthesized using a chemical co-precipitation method and agglomerated using a spray-drying method. DZ40M, a superalloy with a 6 mm thickness and 25.4 mm diameter, was used as a substrate for the TBCs. First, a 100 μm thick bond coat of NiCrAlY (Amdry 9624, Oerlikon Metco, Winterthur, Switzerland) was deposited on the substrates using the PS-PVD technique. Next, the YSZ layer was deposited on the bond coat to generate the underlying ceramic layer. Subsequently, a GYbZ ceramic layer was deposited on the YSZ layer to prepare the top ceramic layer. To obtain a gas-phase deposited quasi-columnar coating of GYbZ, the spraying distances of 600, 800, and 1000 mm were employed. Table 1 lists the deposition parameters of the TBCs.

Table 1. The spray parameters of the GYbZ/YSZ DCL TBCs.

	Current (A)	**Flow Rate (L·min^{-1})**					**Feed Rate (g·min^{-1})**	**Spraying Distance (mm)**
		Ar	He	H_2	O_2	Carrier gas		
Bond coat	1650	110	–	6	–	6	30	450
YSZ layer	2600	–	60	–	2	10	2 × 5	1000
GYbZ layer	2600	–	60	–	–	10	2 × 2.5	600, 800, and 1000

2.2. Performance Evaluation

The microstructures of the GYbZ agglomerated powders and TBCs were characterized using an FE-SEM (Nova-Nono430, FEI, Hillsboro, OR, USA). The chemical composition of the GYbZ agglomerated powders was examined using X-ray fluorescence spectrometry

(XRF) (Axios FAST, PANalytical, Almelo, The Netherland), and the particle size of the GYbZ agglomerated powder was measured using a laser scattering particle size analyzer (Mastersizer-3000, Malvern PANalytical, Shanghai, China). Moreover, the flowability of the powders was indirectly measured using the Hausner ratio (H). According to Chinese national standards, GB/T 5162-2006 and GB/T 1479.1-2011, the tap density (ρ_T) and bulk density (ρ_B) of the agglomerated powders, were measured and the H was calculated as $H = \rho_T / \rho_B$.

X-ray diffraction (XRD) (D/max 2550PC, Rigaku Ltd., Tokyo, Japan) studies were performed for exploring the structural phase of the GYbZ coating. In addition, nano-indentation (NHT2, Anton Paar, Graz, Austria) was used to determine the Vickers hardness and Young's modulus of the ceramic coatings. Each sample had ten or more effective indentations, and their average value was recorded. The thermal shock resistances of GYbZ/YSZ DCL TBCs were assessed using water-quenching tests. All samples were first heated at 1100 °C in a furnace for 10 min and then direct water quenching was performed to cool them down to room temperature. This process was repeated until visible spallation occurred on the coating's surface or the substrates deformed.

3. Results

Figure 1a,b show SEM micrographs of GYbZ agglomerated powders. Most agglomerated powders exhibit an intact spherical appearance compared with commercial 7YSZ powders [21]. The agglomerated powders primarily consist of micron-sized GYbZ particles with irregular shapes that were loosely compacted (Figure 1b). Agglomerated powders with an incompact structure can promote the evaporation of powders, and the spherical structures can improve the fluidity of GYbZ agglomerated powders to meet the uniform and stable powder-feeding requirements of the PS-PVD technique.

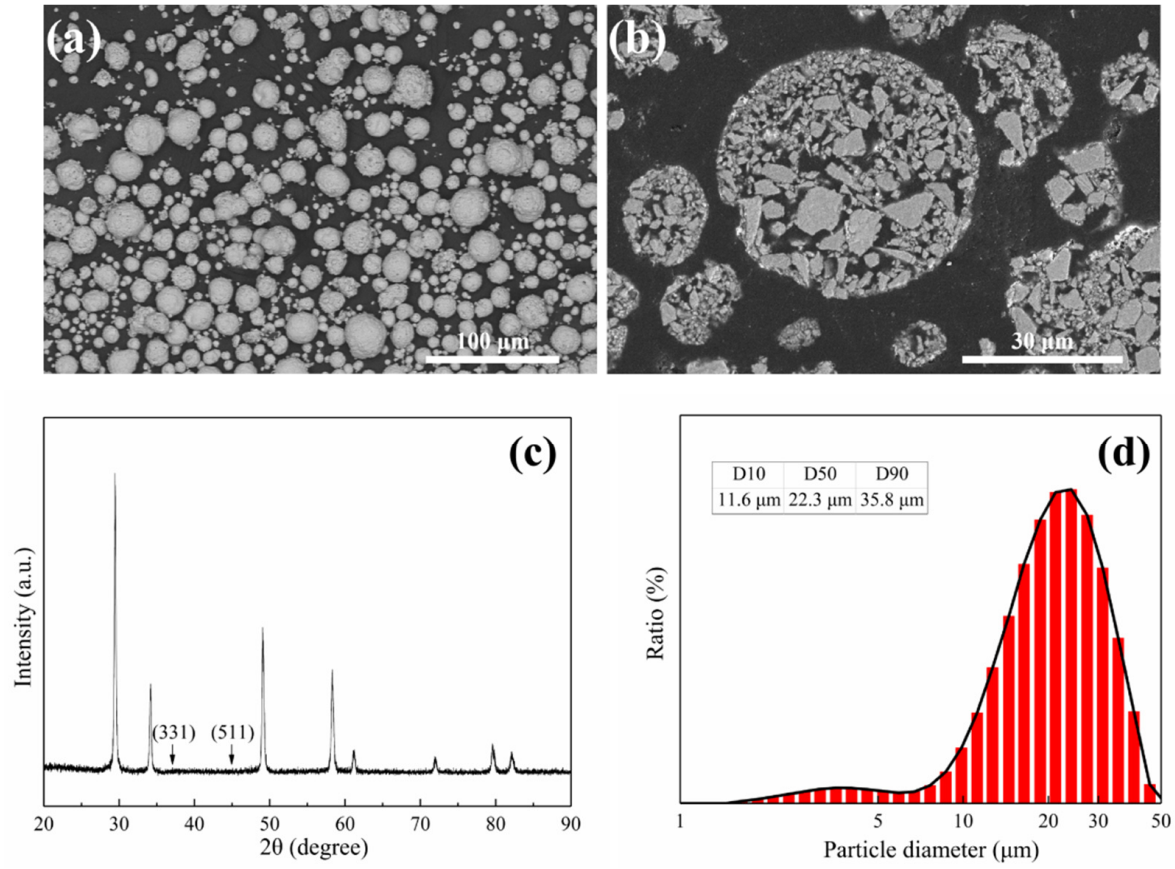

Figure 1. Surface morphology (**a**), cross-sectional morphology (**b**), XRD pattern (**c**), and particle size distribution (**d**) of $(Gd_{0.9}Yb_{0.1})_2Zr_2O_7$ agglomerated powders.

Table 2 presents the XRF compositional analysis results of the GYbZ agglomerated powders. The elemental composition of GYbZ agglomerated powders is close to their theoretical stoichiometric ratio. In addition, there are no superlattice peaks corresponding to the (331) and (511) planes in the XRD patterns shown in Figure 1c, implying that the powder exhibits a fluorite phase. The particle size distribution of GYbZ agglomerated powders is shown in Figure 1d. The powder proportions a particle diameter less than 11.6, 22.3 and 35.8 μm were 10, 50 and 90%, respectively. In the spraying process, powder with a small particle size had low fluidity and powder with a large particle size had a low evaporation rate in the plasma jet. For the GYbZ agglomerated powders, the average particle size was 23 μm, which is appropriate for the PS-PVD technique for coatings [22]. For tap density ρ_T = 1.25 g/cm^3 and bulk density ρ_B = 1.02 g/cm^3, H = 1.23. When H is less than 1.25 [23], the powder has superior fluidity and does not block the powder-feeding pipe.

Table 2. The composition of $(Gd_{0.9}Yb_{0.1})_2Zr_2O_7$ agglomerated powders (in Atomic %) obtained by XRF.

Gd	Yb	Zr	O
10.33	1.30	12.42	75.95

Figure 2 displays the XRD patterns of the GYbZ ceramic layer prepared with different spraying distances. The coatings prepared using the PS-PVD technique exhibited a fluorite phase. In addition, the distribution of XRD peaks is similar to that observed for GYbZ agglomerated powders (Figure 1c), indicating that there was no preferential growth phenomenon in the GYbZ coatings prepared using the PS-PVD technique.

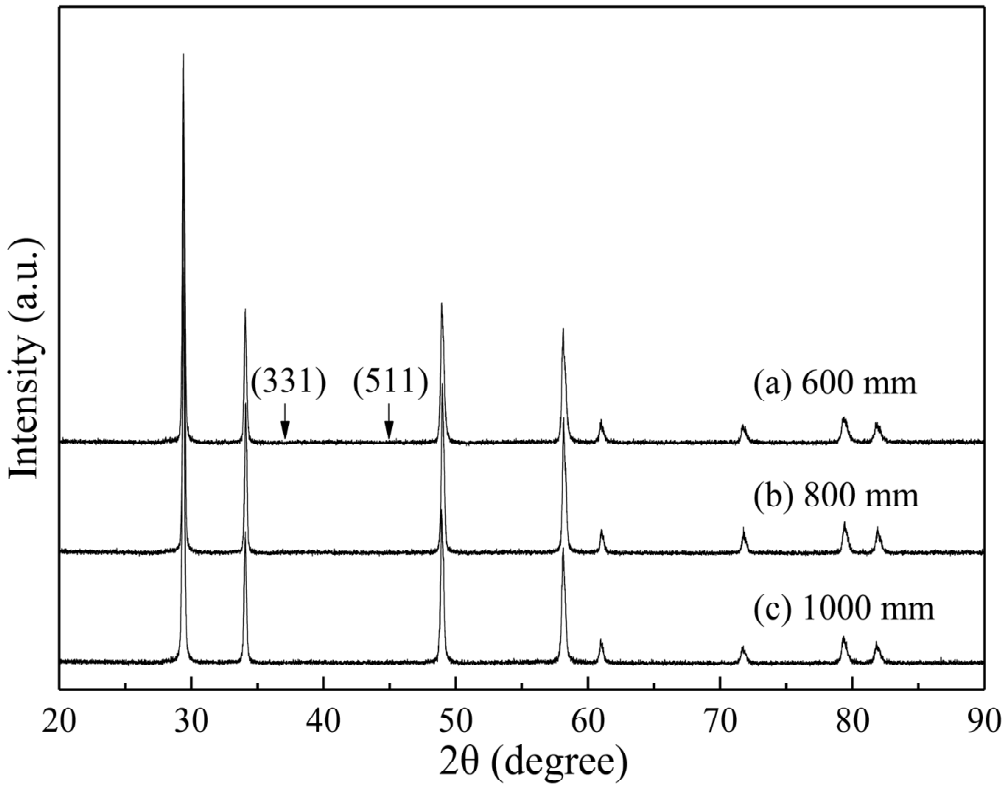

Figure 2. XRD patterns of the GYbZ ceramic layer prepared with a spraying distance of (**a**) 600, (**b**) 800, and (**c**) 1000 mm.

Figure 3 exhibits the surface micrographs of the GYbZ/YSZ DCL TBCs prepared with various spraying distances. Significant differences in the surface structures of GYbZ

coatings are observed. Figure 3a shows the GYbZ coating prepared with a spraying distance of 600 mm. The areas are closely connected, with no obvious gaps. On further magnification, a microstructure framework comprising closely packed columnar crystals is observed (Figure 3(a1)). However, the inter-columnar gaps are filled with unmelted components, which exhibit the characteristics of a closely packed columnar structure [24]. The GYbZ coating prepared with an 800 mm spraying distance has a typical quasi-columnar surface structure, where the columnar crystals are uniformly distributed and separated by inter-columnar gaps (Figure 3b). On further magnification (Figure 3(b1)), the top of the columnar crystals has a hemispherical structure, which is described as a cauliflower-like appearance of coatings prepared by the PS-PVD technique [25]. In comparison, the distribution of columnar crystals in the GYbZ coating prepared with a spraying distance of 1000 mm is denser, and the inter-columnar gaps are narrower (Figure 3c). When the magnification is increased (Figure 3(c1)), the size of cauliflower-like appearance at the top of columnar crystals is significantly reduced compared with that shown in Figure 3(b1).

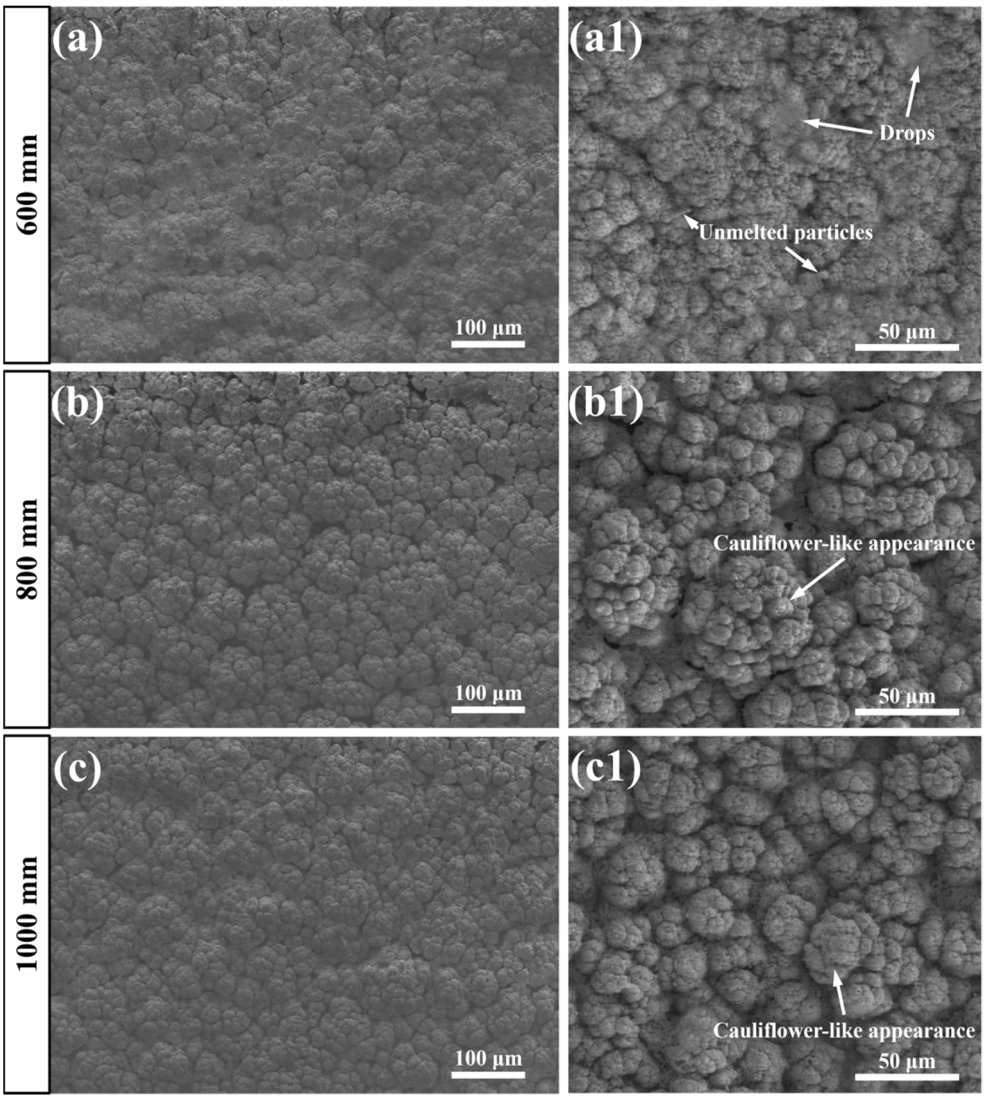

Figure 3. SEM images of the surface of GYbZ/YSZ DCL TBCs prepared with spraying distances of (**a**,**a1**) 600, (**b**,**b1**) 800, and (**c**,**c1**) 1000 mm.

Figure 4a–c shows the cross-sectional morphologies of GYbZ/YSZ DCL TBCs, where the columns have a thickness of 210–250 μm and the thickness ratio of GYbZ:YSZ is about 1:3. The thickness of TGO at the interface between the bond coat and ceramic layer is

approximately 0.6 µm, with no correlation with the spraying distance. The GYbZ ceramic layers prepared with varying spraying distances exhibited different microstructures. This is because of the apparent reduction in the plasma temperature and increase in the evaporation degree of powder with increasing spraying distance [26]. The agglomerated powders first change from a droplet to vapor and then to condensed particles [27], resulting in various deposition patterns at different spraying distances.

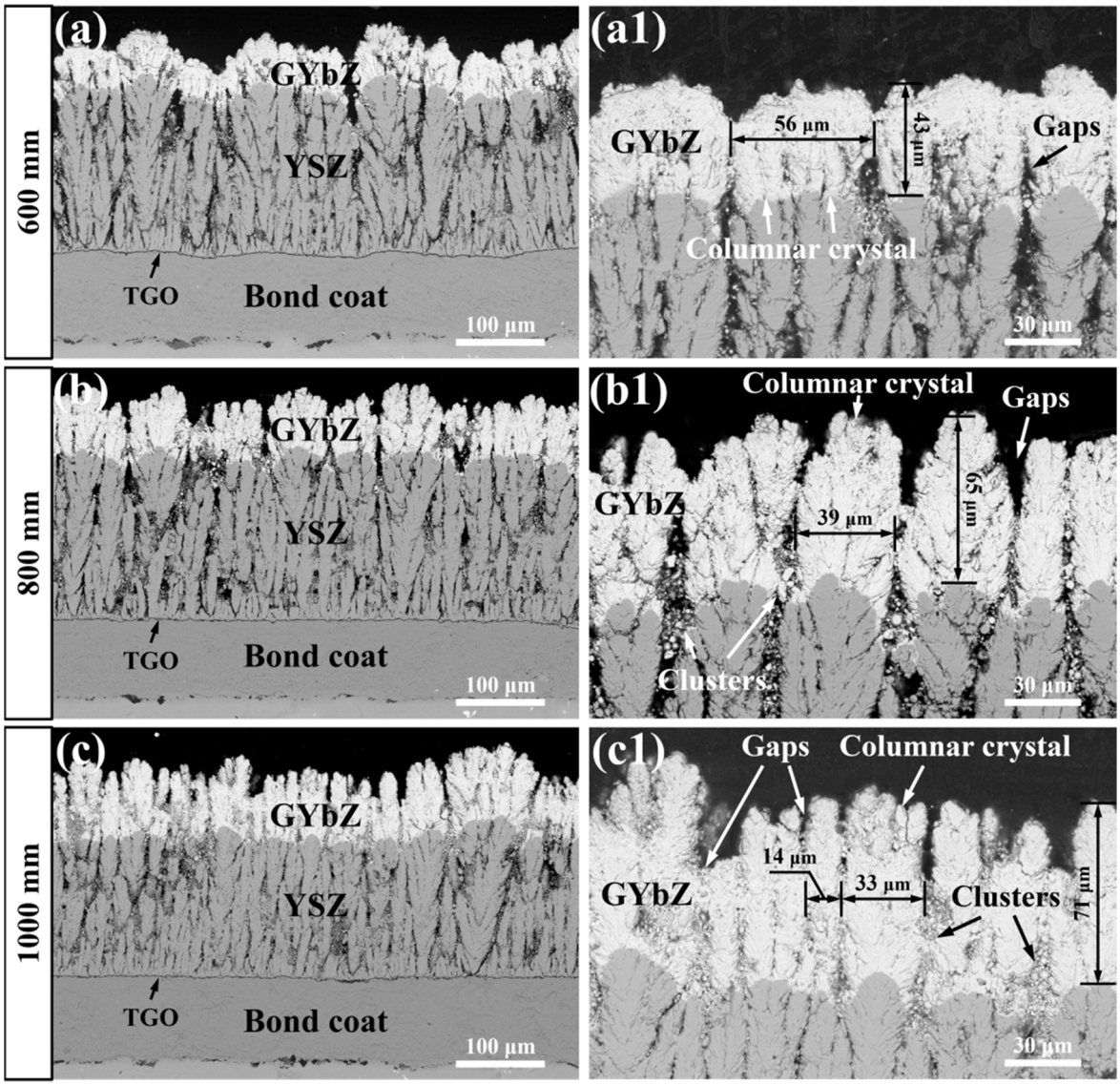

Figure 4. Cross-sectional SEM image of the GYbZ/YSZ DCL TBCs prepared with spraying distances of (**a**,**a1**) 600, (**b**,**b1**) 800, and (**c**,**c1**) 1000 mm.

The GYbZ coating prepared with a 600 mm spraying distance showed a closely packed columnar structure [28]. The thickness of the GYbZ coating, as shown in Figure 4a, is about 43 µm and thinner than the other coatings (which are about 65 and 71 µm). This is due to the inhibition of the growth of columnar crystals by molten droplets. As can be seen in Figure 4(a1), the lower part of the GYbZ coating is still in the columnar structure and separated by inter-columnar gaps, but the columnar crystals at the top of coating are connected due to the inter-columnar gaps filled with molten droplets. Therefore, the closely packed columnar structure results from the co-deposition of liquid splats and vapors of powders.

When the spraying distance is increased to 800 and 1000 mm, the GYbZ coatings showed the quasi-columnar structure (Figure 4b,c). As mentioned in the introduction, this structure is attractive for TBCs owing to its excellent thermal cycling and insulation performance. Several clusters can be observed in Figure 4(b1,c1), and they may result from the homogeneous nucleation of the gas phase or the unmelted particles [29,30]. Figure 4(b1) exhibits the GYbZ coating prepared with a spraying distance of 800 mm, and the cross-section of columnar crystals has a feather-like appearance. In addition, the width of columnar crystals is about 39 μm with well-developed dendrites, and the inter-columnar gaps are obvious and filled with parts of clusters. In contrast, the width of columnar crystals in the GYbZ coating prepared with a spraying distance of 1000 mm, shown in Figure 4(c1), has generally narrowed. Moreover, large areas of the inter-column gaps are filled with clusters, which may reduce the strain tolerance and enhance the risk of failure during thermal cycling [31]. The reason for these structural differences is that the temperature gradient at the front of the substrate's surface is higher when the spraying distance is 800 mm than when the spraying distance is 1000 mm. Thus, the columnar crystals are more likely to grow (with dendrites) by adsorbing the gas-phase particles [32]. Moreover, due to the shadowing effect [33], the growth of grains in inter-column gaps when the spraying distance is 800 mm is inhibited, resulting in the formation of typical quasi-columnar structures prepared using the PS-PVD technique.

The Young's modulus and Vickers hardness of the GYbZ/YSZ DCL TBCs are listed in Table 3. The GYbZ layer prepared with a 600 mm spraying distance exhibited the highest H_v and E, which significantly decreased when the spraying distance was increased to 800 mm. With a further increase in the spraying distance, the H_v and E of the GYbZ layer slightly decreased. Based on these results, we conclude that the H_v and E can be improved by reducing the spraying distance. This is mainly because reducing the spraying distance increases the matrix temperature, which affects the process of crystallization. In addition, the presence of molten droplets at a spraying distance of 600 mm also improves the H_v and E of the GYbZ layer. Generally, the top ceramic layer does not require a high Young's modulus, which is associated directly with decreasing the TBCs' strain tolerance [34], and they are more likely to crack under high stress. However, a high level of hardness can enhance the erosion and wear resistance of the coating to foreign particles.

Table 3. The Young's modulus (E) and Vickers hardness (H_v) of the TBCs.

Layer	Spraying Distance	H_v (GPa)	E (GPa)
GYbZ	600 mm	11.22 ± 0.79	175.94 ± 25.03
GYbZ	800 mm	7.21 ± 0.16	119.86 ± 10.37
GYbZ	1000 mm	5.83 ± 0.28	100.28 ± 13.2
YSZ	–	10.44 ± 0.34	132.57 ± 10.68

The thermal shock resistance of the GYbZ/YSZ DCL TBCs prepared with various spraying distances was evaluated after 200 cycles of the water-quenching tests between 1100 °C and RT (~30 °C). The TBCs demonstrated excellent thermal shock resistance compared with those reported in previous studies. GZO SCL TBCs and GZO/YSZ DCL TBCs were reported to have failed after 40 cycles of water-quenching tests and the DCL TBCs had better thermal shock resistance than SCL TBCs [35]. Even YSZ SCL TBCs with excellent thermal shock resistance showed visible failure after 160 cycles of water-quenching tests [36]. The same water-quenching test conditions and coating preparation method in the above studies were adopted here, and the excellent thermal shock resistance of the GYbZ/YSZ DCL TBCs is primarily ascribed to the modifications in the PS-PVD spraying process and the superior high-temperature performance of doped GYbZ coatings.

Among these three coatings, shown in Figure 5, the GYbZ coating prepared with an 800 mm spraying distance exhibited the best thermal shock resistance, as shown in Figure 5f–j. First, a few caves randomly distributed in the coating surface were observed af-

ter 50 cycles of water-quenching tests (Figure 5g). As the water-quenching tests progressed, the number of caves in the coating surface was not observed to increase. This failure pattern was observed in all three coating surfaces, and the failure process is consistent. Then, after 200 cycles of water-quenching tests, exfoliation appeared sporadically at the center of the coating surface (Figure 5j). In comparison, the GYbZ coating prepared at a spraying distance of 1000 mm is more likely to fail during the water-quenching tests (Figure 5k–o). Except for the caves appearing after 50 cycles of water-quenching tests, exfoliation was observed at the center of the coating surface after just 150 cycles of water-quenching tests (Figure 5n). With an increase in the water-quenching time, the exfoliation was observed to expand rapidly, finally connecting to large areas (Figure 5o). In addition, some delamination cracks could be observed at the circumference of the coating after 200 cycles of water quenching.

The GYbZ coating prepared with a 600 mm spraying distance showed the worst thermal shock resistance in water-quenching tests (Figure 5a–e). First, curling can be observed at the edge of the as-sprayed coatings. This is mainly because the deposition temperature increased by approximately 500 °C when the spraying distance was decreased from 800 to 600 mm. Especially at the circumference of the coating, the stress is relatively concentrated. After several water-quenching cycles, the curled parts spalled off from the coating surface, forming the spalled areas. The obvious spalled areas can be observed in Figure 5b, and they will expand slowly with the increasing water-quenching times. After 50 cycles of water-quenching tests, caves were also found in the coating surface. In addition, exfoliation occurred in the coating surface after 100 cycles of water-quenching tests (Figure 5c), which was the earliest among other coatings and had the largest failure areas at the same stage among all three coatings. Finally, after 200 cycles of water-quenching tests, a large area of exfoliation and spallation and several radiate cracks were observed in the coating surface.

After 200 cycles of water-quenching tests, the main failure patterns in the surface of the GYbZ/YSZ DCL TBCs can be classified into the following five types: caves, exfoliation, delamination cracks, spalled areas, and radiate cracks. Figure 6a shows the main failure pattern of the coating prepared with a spraying distance of 800 mm after water-quenching tests. These patterns are caves and exfoliations. The surface morphology of caves is shown in Figure 6b, and the diameter of these caves is more than 100 μm, which exceeds the general diameter of a cauliflower-like appearance. Meanwhile, these caves are too deep to determine the chemical compositions. Figure 6(b1) shows the cross-sectional morphology of the cave that was caused by the fracture in the YSZ layer. This may be because of the presence of some cracks in the YSZ layer of the as-sprayed coating. Moreover, the YSZ layer did not easily generate new cracks during the water-quenching tests compared to the GYbZ layer, which explains why the number of caves did not increase rapidly with the increasing water-quenching cycles. When cracks propagated in the root of columnar crystal, most of the columnar crystal grown on it peeled off and the joining columnar crystals were affected and fractured, eventually forming caves.

The main failure patterns of the coatings prepared with a spraying distance of 1000 mm after water quenching are caves, delamination cracks, and exfoliation (Figure 7a). The surface morphology of delaminated cracks is shown in Figure 7b, and the chemical composition of the chosen regions are listed in Table 4. Area 'A' consists of Y, Zr, and O, and area 'B' consists of Gd, Yb, Zr, and O. This result indicates that delamination appeared at the YSZ layer and occurred at the circumference of the coatings. The failure process of delamination can be described by the cross-sectional morphology (Figure 7(b1)). In region A on the YSZ coating surface, there is only a small region in GYbZ coating indicating that the GYbZ layer first broke and peeled off from the interface with the YSZ layer. In addition, the delamination cracks were found at the root of YSZ layer, which would result in the fracture of the YSZ coating and peeling out from the root, as shown in region B. The main reason for this failure pattern is the mismatch of thermal expansion coefficient [37], which it is more serious at the circumference of coating due to the stress concentration and leads

to the spallation of the GYbZ layer. Then, the YSZ layer, without the protection of the GYbZ layer, also fractures and peels off from the root after several water-quenching cycles. Thus, this layer-by-layer spallation failure is called delamination of cracks.

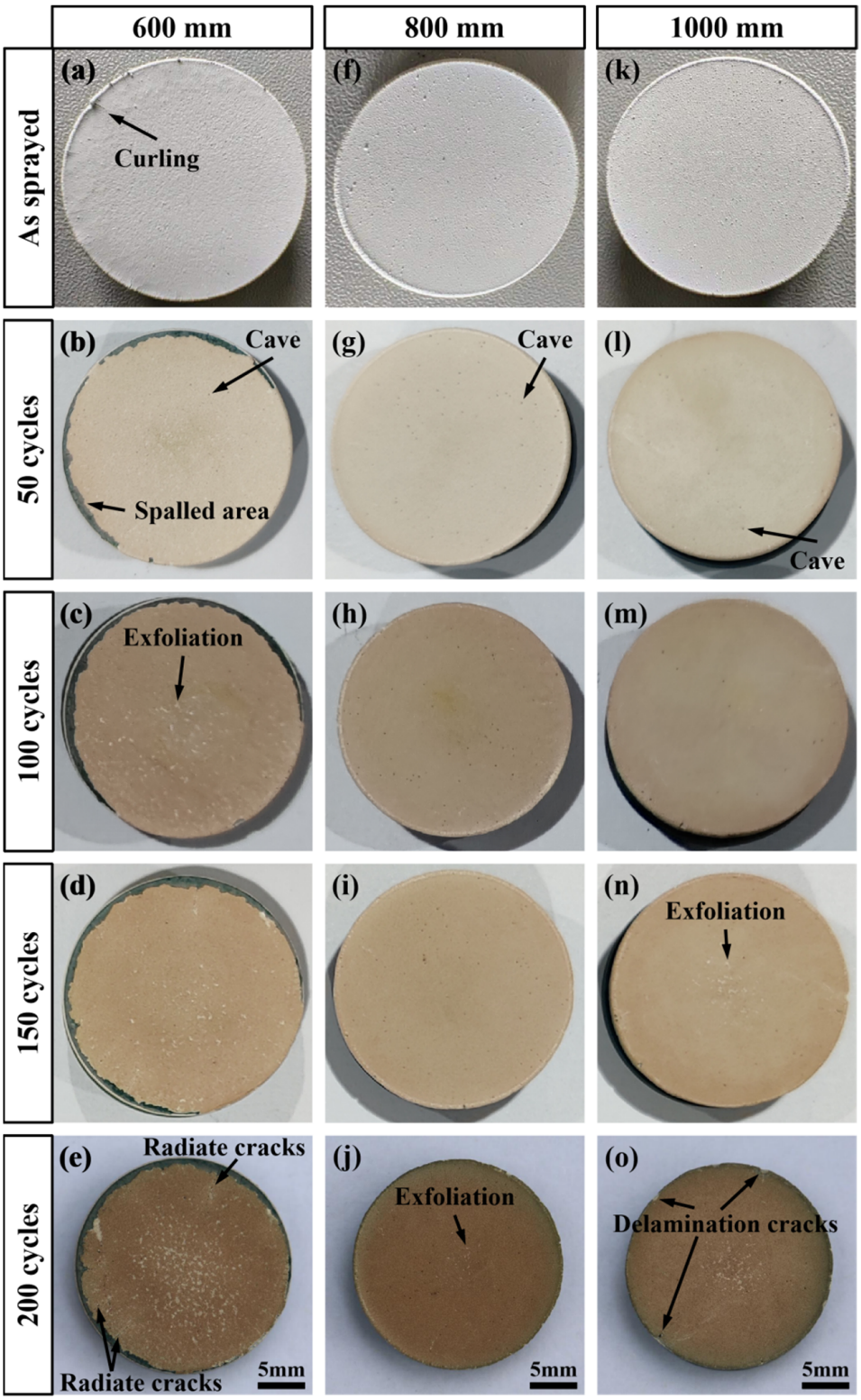

Figure 5. Surface photographs of the GYbZ/YSZ DCL TBCs prepared with spraying distances of (**a**–**e**) 600, (**f**–**j**) 800, and (**k**–**o**) 1000 mm at different stages of water-quenching tests.

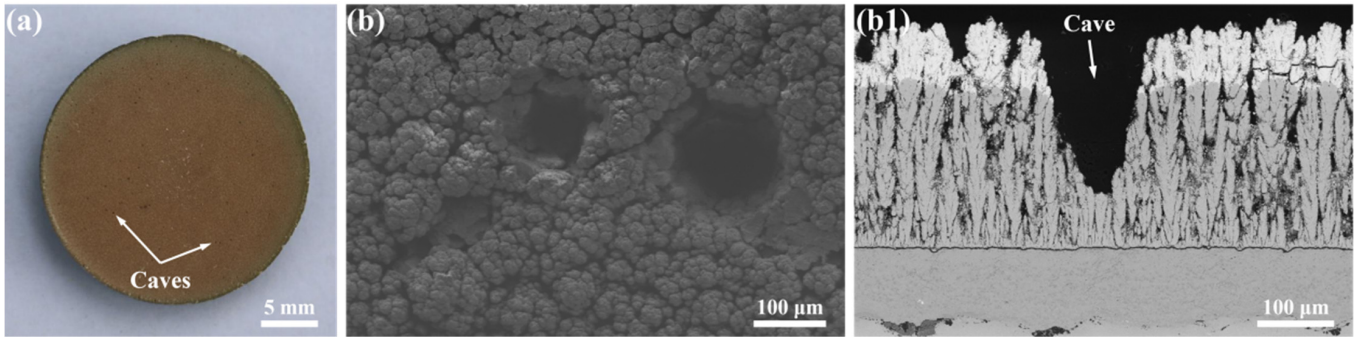

Figure 6. Surface photograph (**a**), surface SEM image (**b**), and cross-sectional SEM image (**b1**) of the GYbZ/YSZ DCL TBCs prepared with a spraying distance of 800 mm after water-quenching tests.

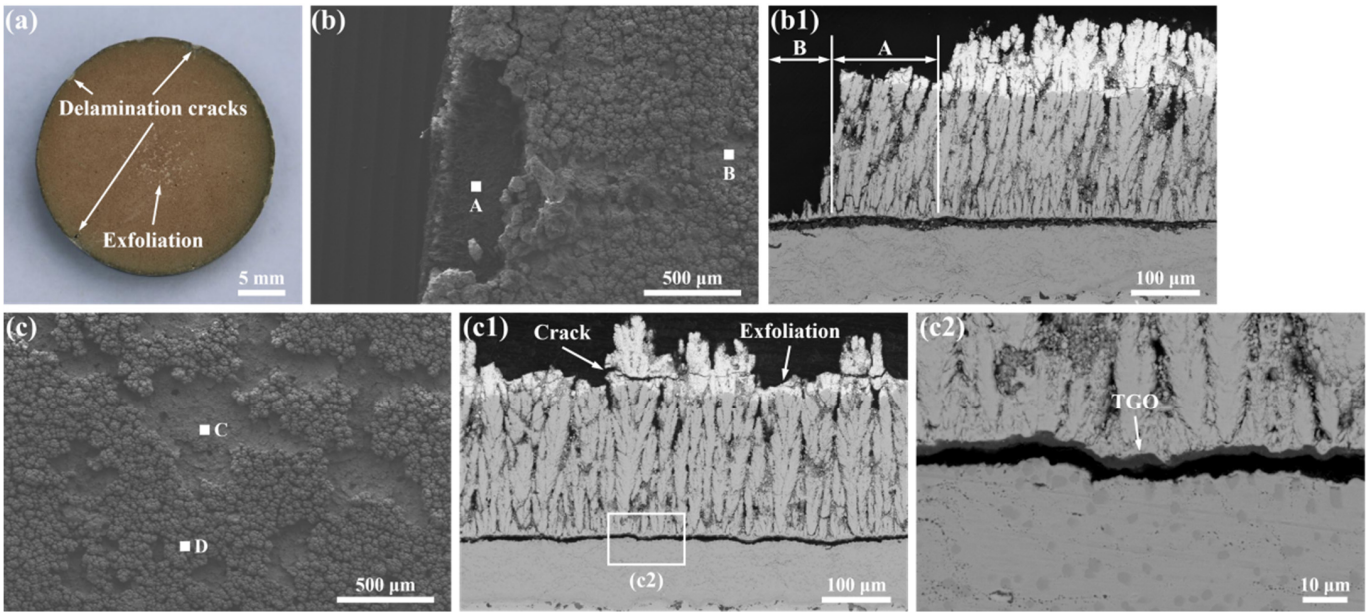

Figure 7. Surface photograph (**a**), surface SEM images (**b**,**c**), and the cross-sectional SEM images (**b1**,**c1**,**c2**) of the GYbZ/YSZ DCL TBCs prepared with spraying distances of 1000 mm after water-quenching tests.

Table 4. The chemical compositions of selected areas in Figures 7 and 8 (in Atomic %).

	Gd	Yb	Y	Zr	O	Ni	Cr	Al
A	–	–	2.02	29.86	68.12	–	–	–
B	11.98	2.62	–	22.65	62.75	–	–	–
C	7.42	0.78	–	18.29	73.51	–	–	–
D	6.01	0.61	–	16.25	77.12	–	–	–
E	–	–	0.54	–	56.29	10.29	10.76	22.12
F	10.74	2.71	–	22.08	64.48	–	–	–

Figure 7c shows the surface morphology of exfoliated surface. Areas 'A' and 'B' constitute Gd, Yb, Zr, and O. The corresponding contents of each element in areas 'A' and 'B' are similar, suggesting that the exfoliation occurred in the GYbZ ceramic layer. In addition, as shown in Figure 7(c1), some obvious cracks exist in the GYbZ layer and the fracture occurred in the middle of several columnar crystals. This indicates that the exfoliation resulted from the crack production and propagation. In fact, except for a small number of cracks occurring in the YSZ layer, most fracture failures occurred in the GYbZ

layer. This is because the fracture toughness of GYbZ (1.11 ± 0.24 MPa·m$^{1/2}$) is lower than YSZ (5.53 ± 0.10 MPa·m$^{1/2}$) [38]. Thus, the cracks were easily propagated in the GYbZ layer. We can consider area of exfoliation as an indicator to assess the GYbZ coatings' thermal shock resistance prepared by various spraying distances due to its occurrence in the GYbZ layer, reflecting the fracture toughness of the coating. The sequence of the thermal shock resistance is 800 > 1000 > 600 mm.

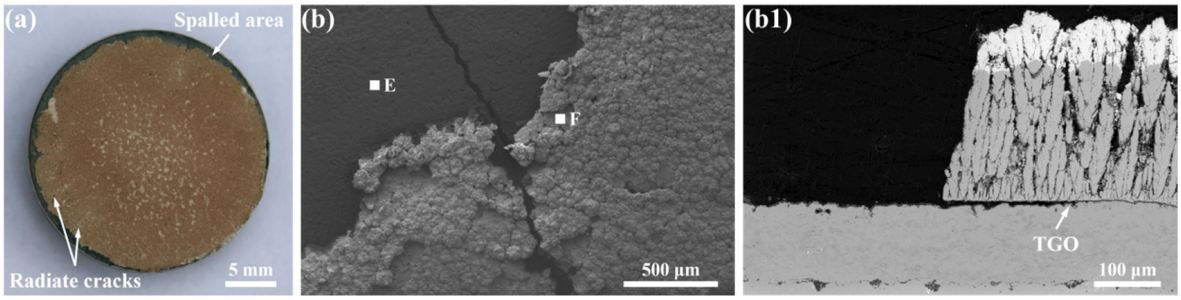

Figure 8. Surface photograph (**a**), surface SEM images (**b**), and the cross-sectional SEM image (**b1**) of the GYbZ/YSZ DCL TBCs prepared with a spraying distance of 600 mm after water-quenching tests.

Figure 7(c2) displays the magnified image of the selected area in Figure 7(c1). The TGO layer is combined with the ceramic layer and a fracture is present at the root of the TGO layer. In general, the growth of the TGO layer accelerated the failure process of TBCs. In this study, the thickness of TGO is rather thin, which increased from approximately 0.6 to 2 μm after 200 cycles of water-quenching tests. In addition, the fracture failure in the TGO layer only occurred at the edge of the coating prepared with spraying distances of 600 and 1000 mm.

Figure 8a shows that the main failure patterns of the coating prepared with a spraying distance of 600 mm after water quenching are caves, exfoliation, spalled areas, and radiate cracks. The surface morphology of the spalled area is shown in Figure 8b. The spallation appeared at the coating circumference. Region 'E' shows the bond coat composition, where the proportion of Al and O is high. It proves that the entire ceramic layer spalled from the coating, but the broken TGO layer remained on the spalled area, which is mainly comprised of Al2O3. For the cross-sectional morphology depicted in Figure 8(b1), the spallation of GYbZ/YSZ DCL occurred in the weakest TGO layer. We can also observe that the curvatures formed by thermal deformation between the ceramic layer and bond coat (substrate) differed. The primary cause of spallation is the curling at the edge of the as-sprayed coating, which resulted in the formation of the spalled areas after several cycles of water quenching. The deformation of the substrate after an excessive number of water-quenching cycles and the mismatch of the thermal expansion coefficient between the bond coat and ceramic layer also led to the expansion of spalled areas. In addition, a few radiate cracks extended inward from the circumference of the coating. Figure 8b shows that the cracks appeared in the ceramic layer and bond coat. All the radiate cracks originated from the substrate, where deformation occurred with cracks after approximately 150 water-quenching cycles.

In general, during the water-quenching cycles, the thermal shock behavior under water quenching can be divided into the following three stages according to the main failure reasons: In the first stage, the failure cause of the TBCs mainly owes to the generation and propagation of cracks. For the GYbZ/YSZ DCL TBCs, cracks are more likely to occur in the GYbZ layer with poor fracture toughness, which leads to exfoliation. However, the formation of caves is considered the result of a few cracks propagated in the YSZ layer of the as-sprayed coating after several cycles of water quenching. In the second stage, the overall failure occurred in the circumference of the coating owing to the stress concentration, and it shows the pattern of delamination cracks. When the failure degree is severe, the spalled areas will appear. In the final stage, because of the substrate deformation, which

occurred after an excessive number of water-quenching cycles, and the mismatch of the thermal expansion coefficient between various layers, the areas of exfoliation and spallation increased rapidly. Simultaneously, the radiate cracks originated from the substrate and then extended inward from the circumference of the coating.

4. Conclusions

We elucidated the influence of spraying distances on the performance and structure of GYbZ coatings prepared by the PS-PVD technique, and their failure behavior is summarized. The GYbZ coating prepared with a spraying distance of 600 mm showed a closely packed columnar structure. However, the coating deposited with spraying distances of 800 and 1000 mm exhibited quasi-columnar structures, in which the GYbZ coating with an 800 mm spraying distance has the thickest columnar crystals, and the inter-columnar gaps are apparent. In addition, the Young's modulus and Vickers hardness decreased with an increased spraying distance.

After 200 cycles of water-quenching tests, the coating structure with a spraying distance of 800 mm remained relatively intact. The most vulnerable part of the TBCs was the GYbZ layer, in which the cracks easily generated and propagated and caused exfoliation on the coating surface. In addition, the cracks in the YSZ layer of as-sprayed coatings caused fractures in the root of the columnar crystals, eventually forming caves. The delamination cracks and spalled areas first occurred at the circumference of the coating, owing to the stress concentration and the thermal expansion coefficient mismatch between various layers. Finally, the radiate cracks appeared with the substrate deformation.

To conclude, the coating prepared with a spraying distance of 800 mm exhibited a typical quasi-columnar structure and a suitable Young's modulus and hardness. Moreover, it displayed excellent thermal shock resistance.

Looking to the future, in order to obtain an advanced TBC that can finally be applied at an ultra-high temperature, we can optimize the spraying parameters and modify the gadolinium zirconate materials by doping other components to improve the quality of the coating, especially the fracture toughness. Furthermore, it may be effective to adopt the gradient transition base on the double-ceramic-layer structure and redesign the thickness of each ceramic layer to alleviate the mismatch of the thermal expansion coefficient.

Author Contributions: Conceptualization, C.D.; methodology, Z.D.; validation, C.D. and X.Z.; formal analysis, H.Z.; investigation, H.Z.; resources, C.D.; data curation, H.Z.; writing—original draft preparation, H.Z.; writing—review and editing, Z.D. and X.C.; supervision, X.Z.; project administration, C.D.; funding acquisition, C.D. All authors have read and agreed to the published version of the manuscript.

Funding: The research was supported by the projects of the Key-Area Research and Development Programs of Guangdong Province (2019B010936001) and Guangzhou (202007020008); the National Natural Science Foundation of China (52001077); the National Key R&D Program of China (2018YFB1502603); the National Natural Science Foundation of China (52171070); the Open Funds of the State Key Laboratory of Rare Earth Resource Utilization (RERU2021016); the Guangdong Academy of Sciences Project (2021GDASYL-20210302005); the Guangdong Special Plan Local Innovation and Entrepreneurship Team (2019BT02C629); the Guangzhou Science and Technology Project (202007020008); the Special Fund Project of the Guangdong Academy of Sciences (2020GDASYL-20200104028, 2020GDASYL-20200402005); and the Guangzhou Major Projects of Industry-University-Research (IUR) Collaborative Innovation "Surface Treatment and Repair for Key Components of Industrial Gas Turbine (IGT)".

Institutional Review Board Statement: Not applicable.

Informed Consent Statement: Not applicable.

Data Availability Statement: There is no additional data reported in this study to support the results.

Conflicts of Interest: The authors declare that they have no known competing financial interests or personal relationships that could have appeared to influence the work reported in this paper. The funders had no role in the design of the study; in the collection, analyses, or interpretation of data; in the writing of the manuscript; or in the decision to publish the results.

References

1. Pintilei, G.; Crismaru, V.; Abrudeanu, M.; Munteanu, C.; Baciu, E.; Istrate, B.; Basescu, N. The behavior of ZrO_2/20% Y_2O_3 and Al_2O_3 coatings deposited on aluminum alloys at high temperature regime. *Appl. Surf. Sci.* **2015**, *352*, 178–183. [CrossRef]
2. Istrate, B.; Rau, J.V.; Munteanu, C.; Antoniac, I.V.; Saceleanu, V. Properties and in vitro assessment of ZrO_2-based coatings obtained by atmospheric plasma jet spraying on biodegradable Mg-Ca and Mg-Ca-Zr alloys. *Ceram. Int.* **2020**, *46*, 15897–15906. [CrossRef]
3. Padture, N.P.; Gell, M.; Jordan, E.H. Thermal Barrier Coatings for Gas-Turbine Engine Applications. *Science* **2002**, *296*, 280–284. [CrossRef] [PubMed]
4. Evans, A.G.; Clarke, D.R.; Levi, C.G. The influence of oxides on the performance of advanced gas turbines. *J. Eur. Ceram. Soc.* **2008**, *28*, 1405–1419. [CrossRef]
5. Vassen, R.; Cao, X.; Tietz, F.; Basu, D.; Stöver, D. Zirconates as New Materials for Thermal Barrier Coatings. *J. Am. Ceram. Soc.* **2004**, *83*, 2023–2028. [CrossRef]
6. Vassen, R.; Stuke, A.; Stöver, D. Recent Developments in the Field of Thermal Barrier Coatings. *J. Therm. Spray Technol.* **2009**, *18*, 181–186. [CrossRef]
7. Li, S.; He, W.; Shi, J.; Wei, L.; He, J.; Guo, H. PS-PVD gadolinium zirconate thermal barrier coatings with columnar microstructure sprayed from sintered powder feedstocks. *Surf. Coat. Technol.* **2019**, *383*, 125243. [CrossRef]
8. Jiang, T.; Xie, M.; Guan, L.; Wang, X.; Song, X. Effect of Nb^{5+} and Cu^{2+} codoping on thermal properties of $Gd_2Zr_2O_7$ ceramic. *J. Rare Earths* **2020**, *39*, 180–185. [CrossRef]
9. Vassen, R.; Dietrich, M.; Lehmann, H.; Cao, X.Q.; Pracht, G.; Tietz, F.; Pitzer, D.; Stöver, D. Development of oxide ceramics for an application as TBC, Materialwiss. *Werkst* **2001**, *32*, 673–677. [CrossRef]
10. Guo, L.; Guo, H.; Peng, H.; Gong, S. Thermophysical properties of Yb_2O_3 doped $Gd_2Zr_2O_7$ and thermal cycling durability of $(Gd_{0.9}Yb_{0.1})_2Zr_2O_7$/YSZ thermal barrier coatings. *J. Eur. Ceram. Soc.* **2013**, *34*, 1255–1263. [CrossRef]
11. Sampath, S.; Schulz, U.; Jarligo, M.O.; Kuroda, S. Processing science of advanced thermal-barrier systems. *MRS Bull.* **2012**, *37*, 903–910. [CrossRef]
12. Mao, J.; Liu, M.; Deng, Z.; Wen, K.; Deng, C.; Yang, K.; Chen, Z. Coating deposition regularity depended on orientation difference in PS-PVD plasma jet. *Chin. J. Aeronaut.* **2020**, *33*, 3460–3468. [CrossRef]
13. Song, J.; Zhang, X.; Deng, C.; Deng, C.; Liu, M.; Zhou, K.; Tong, X. Research of in situ modified PS-PVD thermal barrier coating against CMAS (CaO–MgO–Al_2O_3–SiO_2) corrosion. *Ceram. Int.* **2016**, *42*, 3163–3169. [CrossRef]
14. Zhang, X.; Song, J.; Deng, Z.; Wang, C.; Niu, S.; Liu, G.; Deng, C.; Deng, C.; Liu, M.; Zhou, K.; et al. Interface evolution of Si/Mullite/Yb_2SiO_5 PS-PVD environmental barrier coatings under high temperature. *J. Eur. Ceram. Soc.* **2019**, *40*, 1478–1487. [CrossRef]
15. Mauer, G.; Vaßen, R. Plasma Spray-PVD: Plasma Characteristics and Impact on Coating Properties. *J. Phys. Conf. Ser.* **2012**, *406*, 012005. [CrossRef]
16. Hospach, A.; Mauer, G.; Vaßen, R.; Stöver, D. Columnar-Structured Thermal Barrier Coatings (TBCs) by Thin Film Low-Pressure Plasma Spraying (LPPS-TF). *J. Therm. Spray Technol.* **2010**, *20*, 116–120. [CrossRef]
17. Goral, M.; Kotowski, S.; Nowotnik, A.; Pytel, M.; Drajewicz, M.; Sieniawski, J. PS-PVD deposition of thermal barrier coatings. *Surf. Coat. Technol.* **2013**, *237*, 51–55. [CrossRef]
18. Rezanka, S.; Mauer, G.; Vaßen, R. Improved Thermal Cycling Durability of Thermal Barrier Coatings Manufactured by PS-PVD. *J. Therm. Spray Technol.* **2013**, *23*, 182–189. [CrossRef]
19. Li, C.; Guo, H.; Gao, L.; Wei, L.; Gong, S.; Xu, H. Microstructures of Yttria-Stabilized Zirconia Coatings by Plasma Spray-Physical Vapor Deposition. *J. Therm. Spray Technol.* **2014**, *24*, 534–541. [CrossRef]
20. Zhang, X.; Zhou, K.; Deng, C.; Liu, M.; Deng, Z.; Song, J. Gas-deposition mechanisms of 7YSZ coating based on plasma spray-physical vapor deposition. *J. Eur. Ceram. Soc.* **2015**, *36*, 697–703. [CrossRef]
21. Zhou, F.; Wang, Y.; Wang, Y.; Wang, L.; Gou, J.; Chen, W. A promising non-transformable tetragonal YSZ nanostructured feedstocks for plasma spraying-physical vapor deposition. *Ceram. Int.* **2018**, *44*, 1201–1204. [CrossRef]
22. Góral, M.; Kotowski, S.; Sieniawski, J. The Technology of Plasma Spray Physical Vapour Deposition. *High Temp. Mater. Process.* **2013**, *32*, 33–39. [CrossRef]
23. Guo, A.; Beddow, J.; Vetter, A. A simple relationship between particle shape effects and density, flow rate and Hausner Ratio. *Powder Technol.* **1985**, *43*, 279–284. [CrossRef]
24. Gao, L.; Guo, H.; Wei, L.; Li, C.; Xu, H. Microstructure, thermal conductivity and thermal cycling behavior of thermal barrier coatings prepared by plasma spray physical vapor deposition. *Surf. Coat. Technol.* **2015**, *276*, 424–430. [CrossRef]
25. Deng, Z.-Q.; Mao, J.; Liu, M.; Deng, C.-M.; Ma, J.-T. Regional characteristic of 7YSZ coatings prepared by plasma spray-physical vapor deposition technique. *Rare Met.* **2021**, *40*, 3308–3315. [CrossRef]

26. von Niessen, K.; Gindrat, M. Plasma Spray-PVD: A New Thermal Spray Process to Deposit Out of the Vapor Phase. *J. Therm. Spray Technol.* **2011**, *20*, 736–743. [CrossRef]
27. Gao, L.; Wei, L.; Guo, H.; Gong, S.; Xu, H. Deposition mechanisms of yttria-stabilized zirconia coatings during plasma spray physical vapor deposition. *Ceram. Int.* **2015**, *42*, 5530–5536. [CrossRef]
28. Zhao, C.; He, W.; Shi, J.; Guo, Q.; Li, J.; Guo, H. Deposition mechanisms of columnar structured $La_2Ce_2O_7$ coatings via plasma spray-PVD. *Ceram. Int.* **2020**, *46*, 13424–13432. [CrossRef]
29. Gao, L.; Guo, H.; Wei, L.; Li, C.; Gong, S.; Xu, H. Microstructure and mechanical properties of yttria stabilized zirconia coatings prepared by plasma spray physical vapor deposition. *Ceram. Int.* **2015**, *41*, 8305–8311. [CrossRef]
30. Zhang, B.; Wei, L.; Guo, H.; Xu, H. Microstructures and deposition mechanisms of quasi-columnar structured yttria-stabilized zirconia coatings by plasma spray physical vapor deposition. *Ceram. Int.* **2017**, *43*, 12920–12929. [CrossRef]
31. Zhang, X.; Zhou, K.; Liu, M.; Deng, C.; Mao, J.; Deng, Z. Mechanisms governing the thermal shock and tensile fracture of PS-PVD 7YSZ TBC. *Ceram. Int.* **2017**, *44*, 3973–3980. [CrossRef]
32. Deng, Z.; Liu, M.; Mao, J.; Deng, C.; Zhang, X. Stage growth of columnar 7YSZ coating prepared by plasma spray-physical vapor deposition. *Vacuum* **2017**, *145*, 39–46. [CrossRef]
33. Mauer, G.; Hospach, A.; Zotov, N.; Vaßen, R. Process Conditions and Microstructures of Ceramic Coatings by Gas Phase Deposition Based on Plasma Spraying. *J. Therm. Spray Technol.* **2012**, *22*, 83–89. [CrossRef]
34. Zhang, X.; Zhou, K.; Liu, M.; Deng, C.; Deng, Z.; Chen, B. Toughness and elasticity behaviors in nano-structured 7 wt.% Y_2O_3-stabilized ZrO_2 coating. *Surf. Coat. Technol.* **2015**, *276*, 316–319. [CrossRef]
35. Zhu, R.-B.; Zou, J.-P.; Mao, J.; Deng, Z.-Q.; Zhang, X.-F.; Deng, C.-M.; Liu, M. A comparison between novel $Gd_2Zr_2O_7$ and $Gd_2Zr_2O_7$/YSZ thermal barrier coatings fabricated by plasma spray-physical vapor deposition. *Rare Met.* **2020**, *40*, 2244–2253. [CrossRef]
36. Zhang, X.; Liu, M.; Li, H.; Deng, C.; Deng, C.; Deng, Z.; Niu, S.; Zhou, K. Structural evolution of Al-modified PS-PVD 7YSZ TBCs in thermal cycling. *Ceram. Int.* **2019**, *45*, 7560–7567. [CrossRef]
37. Zhang, H.; Guo, L.; Ma, Y.; Peng, H.; Guo, H.; Gong, S. Thermal cycling behavior of $(Gd_{0.9}Yb_{0.1})_2Zr_2O_7$/8YSZ gradient thermal barrier coatings deposited on Hf-doped NiAl bond coat by EB-PVD. *Surf. Coat. Technol.* **2014**, *258*, 950–955. [CrossRef]
38. Zhang, Y.; Guo, L.; Zhao, X.; Wang, C.; Ye, F. Toughening effect of Yb_2O_3 stabilized ZrO_2 doped in $Gd_2Zr_2O_7$ ceramic for thermal barrier coatings. *Mater. Sci. Eng. A* **2015**, *648*, 385–391. [CrossRef]